Numerical Simulation of the Lateral Impact on Composite Beams

Torin J. A. Kelderman[1]

University of New South Wales at Canberra

The numerical simulation of lateral impact on composite beams is a LS-DYNA and ANSYS simulation of a FEM of a composite beam being impacted by a steel ball. The increasing use of composites requires a broader understanding of their behaviour especially under different loading conditions. The behaviour of a material under dynamic loading (impact) is a crucial element of using that material in a product (such as car, plane or building) to ensure the safety of the occupants. The simulations are of a clamped composite beam using two different materials – SE-84 GFRP and T300/934 CFRP – being impacted by a steel ball. The simulations modelled previous analytical and experimental data accurately. The simulation was studying the low velocity impact of the composite material and used 3 m/s in this case. The CFRP beam had a maximum displacement of 16.2mm and an impact force of 250N compared to the GFRP beam which had a maximum displacement of 15.5mm and an impact force of 177.3N. The T300/934 CFRRP beam simulation matched the maximum displacement within 10% and the impact force within 10.7% of the comparison analytical and experimental data.

I. Introduction

The analysis of composite materials is increasing in frequency as the material gains popularity in engineering designs. The use of composite aircraft is increasing as seen in Airbus' A380 and A350 as well as Boeing's 787 Dreamliner (Marsh 2005; Quilter 2001). Race car construction is starting to use composites to reduce weight and improve crashworthiness (Bisagni *et al.* 2005; Mamalis *et al.* 1997). The increasing use is resulting in improved manufacturing processes and will likely introduce the use of composites into increasing everyday use. Duflou *et al.* (2009) conducted a study into the environmental impact of composites compared to steel. He said that there was still some improvement in process technology required before CFRP (this was the particular material he studied) becomes more commonly used in the automotive industry. However, composites are likely to be introduced into the industry. Whenever new materials are introduced into a process, research into the effects of this material is needed. The crash impact analysis of this is crucial to maintaining the safety of the automotive industry with composite use. The response of composite plates to dynamic impact is well known and studied (Swanson 1992, Yigit and Christoforou 1998, Khalili, Mittal and Mohammed Panah 2007). The study of composite beams has been less extensively conducted (Yigit and Christoforou 1995b) and still needs further expansion.

A. Motivation and Scope

The motivation for this project was to expand from the impact work done with composite plates to impact on beams (e.g. thicker and longer sections). This will allow for more understanding of analysis of how low velocity impact affects beams that are in car doors (also potentially in aircraft structures as well). The main scope of work done in this area is for composite plates and with more structures being made with composites there is a need to expand that knowledge to beams. There has been a reasonable scope of research into the failure of composite beams under static loading conditions but not under dynamic (or impact) conditions. The simulation of this composite modelling will help to allow the greater use of simulation over more expensive and time consuming use of analytical and experimental data. As such this project is designed to model analytical and experimental data to allow the simulations to be used with greater confidence and understanding of their accuracy in the future.

B. LS-DYNA Overview

This paper will explore the background theory for impact of composite beams to explain how the impact event is calculated. The dynamic analysis will be conducted using LS-DYNA and ANSYS finite element modelling. The LS-DYNA analysis uses explicit dynamic algorithms in conjunction with different material models such as the composite damage model developed by Chang and Chang and the Matzenmiller, Lubliner and Taylor model (MLT

[1] OCDT, School of Engineering & Information Technology. ZEIT4500

model for composites) (Rahman 2013). The Chang and Chang model uses a three stage iterative process to solve dynamic impacts. It analyses the stress distribution (stage one) then finds the failure mode (stage two) and degrades the appropriate material (stage three), it then recalculates the stiffness factors and repeats. The Chang and Chang progressive damage model uses three different failure criteria: tensile fibre failure, matrix cracking (matrix failure in tension) and matrix crushing (matrix failure due to transverse compression and in-plane shearing) (Chang and Chang 1987b). The MLT model uses continuum damage mechanics and is only applicable to shell elements (Matzenmiller *et al*. 1995). This model uses the deformation to create micro cracks in the material. These change the stiffness and introduce damaged parts of the material once the stress has exceeded a calculated value. Damaged parts are not allowed to carry the load in this model and are modelled as a progressive failure of the material.

C. Composite Materials and Impact Problems

The materials used in various previous studies were examined and two were selected for this study. T300/934 CFRP was used by Yigit and Christoforou (1995b) to conduct an analysis of the impact dynamics of composite beams subjected to transverse impact. T300/5208 CFRP was used by Reddy and Reddy (1991) to conduct a linear and non-linear first ply failure analysis of composite laminates subjected to in-plane and transverse loads. AS4/3502 graphite epoxy pre-impregnated tape was used by Kim *et al.* (1995) in progressive failure analysis of laminated composite beams under static loading of layer-wise constant shear. Santiuste *et al*. (2010) used both the T300/914 CFRP and the AS4/3501-6 CFRP to conduct a comparison of the progressive-failure criteria in the prediction of the dynamic bending failure of composite laminated beams. The GFRP SE84 was used by Mines and Alias (2002) to conduct progressive collapse of polymer composite sandwich beams under static loading. The properties used for the steel sphere was sourced from Khalili *et al.* (2007 pp.265).

D. Dynamic Analysis

Tan and Sun (1985) and Yigit and Christoforou (1995b and 1998) use Hertzian contact law to conduct an analysis of laminate composite plates and beams. Hertzian contact law is explained below. This contact law can be linearized with a reasonable degree of accuracy to enable easier analytical calculations. Hertzian contact law can be expanded to include more accurate assumptions for anisotropic bodies as shown by Khalili *et al.* (2007) and Sveklo (1964). Yigit and Christoforou (1995b) normalized (conducted a non-dimensional analysis) to find a non-dimensional constant that governs the contact between a spherical impactor and laminated composite beam. Since the results will be compared against the results from Yigit and Christoforou (1995b and 1998) and Tan and Sun (1985), the theory of Hertzian contact law will be introduced to enable comparison.

1. Hertzian Contact Law

For low velocity impacts the contact models use Hertzian contact law (Johnson 1985, Tan and Sun 1985). Hertzian contact law is a three phase model: phase one elastic loading, phase two elastic-plastic loading and phase three elastic unloading. The following equations describe these three phases:
Elastic loading:

$$F(\alpha) = K_h \alpha^{3/2} \qquad 0 \le \alpha \le \alpha_y \tag{1}$$

Elastic-plastic loading:

$$F(\alpha) = K_y(\alpha - \alpha_y) + K_h \alpha^{3/2} \qquad \alpha_y \le \alpha \le \alpha_m \tag{2}$$

Elastic unloading:

$$F(\alpha) = K_y(\alpha_m - \alpha_y) + K_h(\alpha^{3/2} - \alpha_m^{3/2} + \alpha_y^{3/2}) \tag{3}$$

where K_h is the Hertzian stiffness; α_y is the critical indentation for 'local yield' to occur; K_y is the linear stiffness of the elastic-plastic loading phase; and α is the local indentation defined as the difference between the displacement of the impactor ($w_i(t)$) and the deflection of the beam ($w(c,t)$) at the contact point .

$$K_h = \frac{4}{3}\sqrt{R}E^* \tag{4}$$

$$\frac{1}{E^*} = \frac{1-\upsilon_1^2}{E_x} + \frac{1}{E_z} \tag{5}$$

$$\alpha_y = \frac{2.72 S_u^2 \pi^2 R}{E^{*2}} \tag{6}$$

$$K_y = 1.5 K_h \sqrt{\alpha_y} \tag{7}$$

$$\alpha(t) = w_i(t) - w(x_c, t) \tag{8}$$

where Ez is the transverse Young's modulus; υ_1 and E_x is the Poisson Ratio and Young's modulus of the impactor respectively; S_u is the transverse (xz) shear strength of the laminate and R is the spherical radius in contact with a flat surface (Johnson 1985).

Since it is difficult to achieve an analytical solution for an impact event using Hertzian contact law, a contact stiffness linearization method was developed by Bucinell *et al.* (1991). This method calculates the equivalent linear stiffness for a single degree-of-freedom lumped model which results in the same maximum contact force. This linearization is inadequate when the details of the contact law are important (Yigit and Christoforou 1995b). In this case each phase (as shown in Eqs. 1, 2, 3) of the contact law can be linearized separately with good results (Yigit and Christoforou 1995a). According to Yigit and Christoforou (1994) damage occurs early in the loading phase and most of the local response is dominated by the second phase of the contact law for composite materials such as the analytical solutions found for the composite beams and plates analysed in Yigit and Christoforou (1995b and 1998) studies. The linearized contact law is shown in Eq. 9:

$$F(\alpha) = K_y \alpha \tag{9}$$

2. Hertz-Sveklo's Theory for elastic contact of two anisotropic bodies

The fundamentals of Sveklo's Theory are the same as Hertzian contact law for isotropic bodies. In isotropic contact the contact patch is circular whereas it is elliptical for orthotropic bodies (Khalili *et al.* 2007 pp. 264). The stiffness parameter K in Hertzian Contact Law (Eq. 1) is given by (Sveklo 1964):

$$\frac{K}{r_s} = \frac{4\pi}{3}(1-\varepsilon^2)^{\frac{3}{8}} \frac{\left[\int_0^{\frac{\pi}{2}} \sum_{j=1}^{2} \sum_{k=1}^{3} Re \frac{\Delta_{kj}^{(3)} \Delta_{kj}}{\Delta_{0j}} \frac{d\theta}{(1-\varepsilon^2 \sin^2\theta)^{\left(\frac{3}{2}\right)}}\right]^{\frac{1}{2}}}{\left[\int_0^{\frac{\pi}{2}} \sum_{j=1}^{2} \sum_{k=1}^{3} Re \frac{\Delta_{kj}^{(3)} \Delta_{kj} d\theta}{\Delta_{0j} \quad \Delta}\right]^{\frac{3}{2}}} \tag{10}$$

$$\Delta = \sqrt{\frac{a}{b}(1-\varepsilon^2 \sin^2\theta)} \tag{11}$$

where ε is the eccentricity of the contact patch ellipse; a is the semi-major axis of the ellipse of the contact area; and b is the semi-minor axis of the ellipse of the contact area (Khalili 1992). These parameters can be found using the following Eqs. 12 and 13 as described in Khalili *et al.* (2007):

$$\int_0^{\frac{\pi}{2}} \sum_{j=1}^{2} \sum_{k=1}^{3} Re \frac{\Delta_{kj}^{(3)} \Delta_{kj}}{\Delta_{0j}} \left(\cos^2\theta - \frac{R_y}{R_x}\sin^2\theta\right) \frac{d\theta}{(1-\varepsilon^2 \sin^2\theta)} = 0 \tag{12}$$

$$\frac{a^3}{F} = \frac{3 r_s}{4\pi} \int_0^{\frac{\pi}{2}} \sum_{j=1}^{2} \sum_{k=1}^{3} Re \frac{\Delta_{kj}^{(3)} \Delta_{kj}}{\Delta_{0j}} \frac{d\theta}{(1-\varepsilon^2 \sin^2\theta)^{\left(\frac{3}{2}\right)}} \tag{13}$$

where r_s is the radius of the impactor; R_y is the radius of the ellipse in the y axis; R_x is the radius of the ellipse in the x axis; and F is the contact force.

3. Normalisation

Yigit and Christoforou (1995b) conducted a non-dimensional analysis of the transverse impact of a spherical steel impactor on a composite beam to create the analysis which is a comparison study for the simulations. This dynamic impact number governs the initial impact response of the beam until the stress waves are reflected back from the boundaries (e.g. the clamped ends). This dynamic impact number contains all the physical parameters of the impact event. This non-dimensional constant is the ratio of inertia effects (the mass ratio μ) to stiffness effects (ε/γ) (Yigit and Christoforou, 1998 pg. 18). They came up with a dynamic impact number in Eq. 14:

$$Dynamic\ Impact\ Number = \left(\frac{\mu}{\varepsilon/\gamma}\right)^{\left(\frac{1}{2}\right)} \quad (14)$$

$$\mu = \frac{M}{m} \quad (15)$$

$$\varepsilon = (12k)^{\frac{1}{2}}\left(\frac{kbG_{xz}}{K_y}\right)\left(\frac{G_{xz}}{E_x}\right)^{\frac{1}{2}} \quad (16)$$

$$\gamma = (12k)^{\frac{1}{2}}\left(\frac{G_{xz}}{E_x}\right)^{\frac{1}{2}}\left(\frac{l}{h}\right) \quad (17)$$

where G_{xz} is the transverse shear modulus; E_x is the Young's modulus; l is the beam length; h is the thickness of the beam; K_y is the linear contact stiffness; M_i is the mass of the impactor; m is the mass of the beam; k is the Mindlin shear correction factor and b is the width of the beam.

II. Methodology:

A. Overall Procedure

The procedure used these steps to create the model: create the geometric model; create the material model; assign the initial velocities; define the parts and contact; assign the material models to the geometric models; define the contact algorithm; define the termination; and define the outputs. The simulation was run using the LS-DYNA Solver and the results were processed using LS-DYNA.

B. The Beam and Sphere Model

The composite beams were created using the LS-DYNA FEM software. The beams were modelled using a 3D solid element (allowing analysis in all three dimensions rather than the '1D' beam element). The beams were set at 2.7mm thick, 20mm wide and 200mm long as per Yigit and Christoforou (1995b). The beam was clamped at both ends modelling a clamped support. The simulation model is shown in figure 1 using the properties in table 1. The beam has 10,000 nodes (10 in the thickness direction, 10 across the width and 100 along the length). The sphere has somewhere in the order of 150 nodes with 10 nodes across the diameter and quadrilateral or triangular elements created from these nodes. The composite laminates used a 10 ply laminate with an arrangement of $[0/+45/90/-45/0]_2$. The initial velocity was set to 3mm/ms as in the experiments in Yigit and Christoforou (1995b).

Table 1: Dimensions of the beam and sphere.

Dimension	Beam	Sphere	Units
Length	200		mm
Width	20		mm
Depth	2.7		mm
Radius		6.35	mm
Initial Velocity		3.0	mm/ms

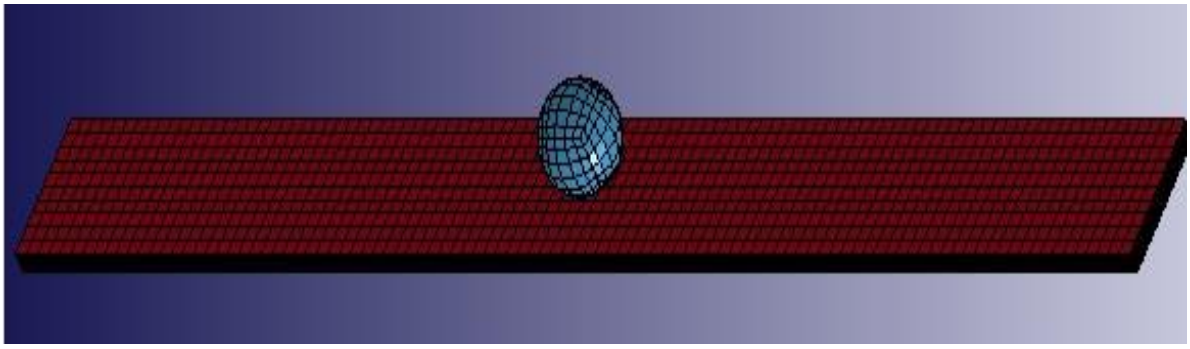

Figure 1: The beam and sphere model.

C. The Material Properties

The composite beam simulation was done using a T300/934 CFRP beam and SE84 GFRP beam. This selection allows a comparison and validation using Yigit and Christoforou (1995b) for the T300/934 CFRP beam. The SE84 GFRP beam can be compared against this work as well for order of magnitude validation. The experimental data found in Sun and Tan (1998) for the T300/934 CFRP plate will also be used to provide order of magnitude

validation for the force during the contact. The mechanical properties used to simulate the models of the two materials are shown in table 2 including the references for where the mechanical properties were taken from. The mechanical properties for the T300/934 CFRP beam were taken from two different sources, the main properties were taken from Yigit and Christoforou (1995b) which is being used as a direct comparison. As the LS-DYNA material models need the strength properties of the materials, which is not supplied in Yigit and Christoforou (1995b), the rest of the mechanical properties were taken from Wu and Springer (1988). They used the same T300/934 CFRP except that the percentage of fibre by volume and arrangement of laminae were not recorded in both papers. Since the arrangements are not the same, the outputs for force and displacement could cause some variation between the simulations to the analytical solution.

Table 2: Mechanical Properties required for the simulation for the T300/934 CFRP beam, SE-84 GFRP beam and the steel impactor.

Property	**T300/934 CFRP beam**	**SE-84 GFRP beam**	**Steel impactor**
E_{xx} (GPa)	120	41	211
E_{yy} (GPa)	7.9	10.3	
G_{xy} (GPa)	5.5	4.0	82.46
G_{xz} (GPa)	5.5	4.0	
υ_{xy}	0.3	0.26	0.28
υ_{xz}	0.3	0.19	
υ_{yz}	0.3	0.19	
ρ (kg/m^3)	1580	1200	7850
Longitudinal tensile strength (MPa)	1778	850	
Longitudinal compressive strength (MPa)	1731	587	
Transverse tensile strength (MPa)	55	31	
Transverse compressive strength (MPa)	294	120	
Transverse shear strength (MPa)	32	77.4	
Interlaminar shear strength (MPa)	101	50	
Reference	Yigit and Christoforou (1995b); Wu and Springer (1988)	Mines and Alias (2002)	Khalili *et al.* (2007 pp. 265)

D. The Material Models

The CFRP and GFRP beams were modelled using three different material models. The first was an orthotropic elastic model, the second was the composite damage model and the third was the composite failure model for solids.

The first material model is an orthotropic elastic model; it defines the material with orthotropic properties and models the behaviour with an entirely elastic response. This model requires only the Young's moduli, shear moduli, Poisson's ratios and densities.

The second model is the composite damage model which uses the three failure criteria as described in Chang and Chang (1987a, 1987b). The three failure modes used are matrix cracking failure criteria; compression failure criteria; and fibre breakage failure criteria (LS-DYNA Theory Manual). The Chang and Chang model uses a three stage iterative process to solve dynamic impacts. It analyses the stress distribution (stage one) then finds the failure mode (stage two) and degrades the appropriate material (stage three), it then recalculates the stiffness factors and repeats.

The third model is the solid composite failure material model which models the composite as an elasto-plastic material. It uses three failure criteria the first of which is an ellipsoidal failure surface. This is governed by Eq. 18 (Schweizerhof *et al.* 1998):

$$f = \frac{4\left(\sigma_1 - \frac{X_t - X_C}{2}\right)^2}{(X_t - X_C)^2} + \frac{4\left(\sigma_2 - \frac{Y_t - Y_C}{2}\right)^2}{(Y_t - Y_C)^2} + \frac{\sigma_{12}^2}{S_C^2} + \frac{\sigma_{13}^2}{S_C^2} + \frac{\sigma_{23}^2}{S_C^2} - 1 \qquad (18)$$

where f is the failure criteria value which determines failure when the value is greater than one; X_t is the tensile strength in the x direction; X_C is the compressive strength in the x direction; Y_t is the tensile strength in the y direction; Y_C is the compressive strength in the y direction; and S_C is the shear strength. The model also uses

failure methods in tension and failure with time step size limits which are based on limiting strains (tensile, compressive and effective). If the element fails in either of these modes it is removed from the following analysis.

E. The contact impact algorithm

The contact used was automatic surface to surface. This contact defines a slave and master surface and the contact-impact algorithm is initiated if a node from one element penetrates the surface of the other element. It creates a resisting force to oppose and eliminate the penetration. From here the contact-impact algorithm will define the equations of state for all the nodes in each element. It will calculate the force, then acceleration, velocity and displacement. It will also calculate the stresses on each node. This is important for the composite damage model; if the stress exceeds the materials strength it will degrade the material properties for the next time steps calculation. The calculation of stresses is also important for the composite failure model to allow calculation of the ellipsoidal failure surface.

F. The Outputs

The two main outputs that will be compared are the beam displacement and impact force versus time; they allow the best comparison to the analytical and experimental results of Yigit and Christoforou (1995b and 1998) and Tan and Sun (1998). These results will be calculated for both the CFRP and GFRP beams and also compared against each other.

III. The Results and Discussion:

A. T300/934 CFRP Beam

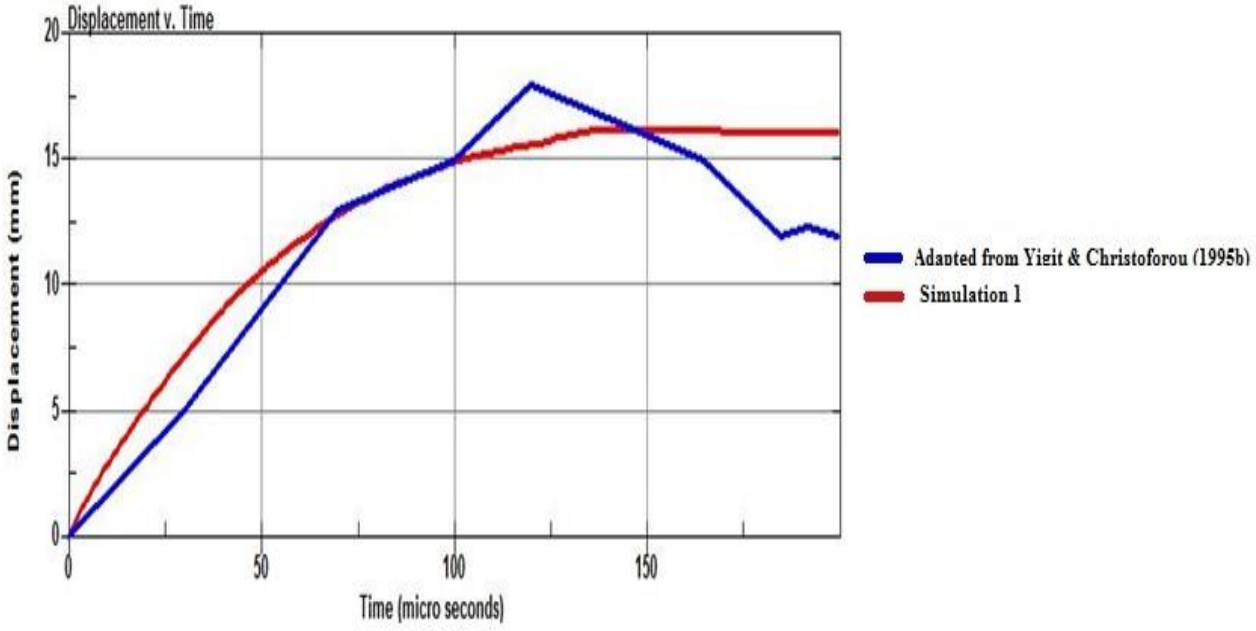

Figure 2: The displacement versus time curve comparing my simulation for the T300/934 CFRP beam to the data adapted from Yigit and Christoforou (1995b).

Figure 2 shows the comparison of the simulation for the T300/934 as compared to the analytical results found by Yigit and Christoforou (1995b). The three different models show very similar curves for the behaviour of the displacement. In figure 2 only the curve from the orthotropic elastic simulation is shown (simulation 1). The analytical results gave a maximum displacement of 18mm whereas the simulation gave a maximum of 16.2mm. The difference between the simulation and the analytical results is 10%. The difference between my simulation results and the analytical results found by Yigit and Christoforou (1995b) can be partially attributed to using the strength of the material from the paper by Wu and Springer (1988). Due to the fibre volume percentage and the exact arrangement of laminae not being published in both the papers there is no certainty that the epoxy – carbon fibre mixture and structure is exactly the same. However, using the strengths from Wu and Springer (1988) was required as the strengths were not published in Yigit and Christoforou (1995b). The mechanical properties of the steel sphere were taken from Khalili *et al*. (2007) which may have resulted in a marginally different weight and strength for the steel in the simulation compared to the steel used in the analytical solution. The different steel properties combined with the differences in the composite material properties can explain the difference between the analytical solution and the simulation. The other difference in the two curves, is that the analytical model

predicts the restoring behaviour of the material before the simulation starts to model it. It started to occur at the 165 microsecond in the simulation but only by a marginal amount.

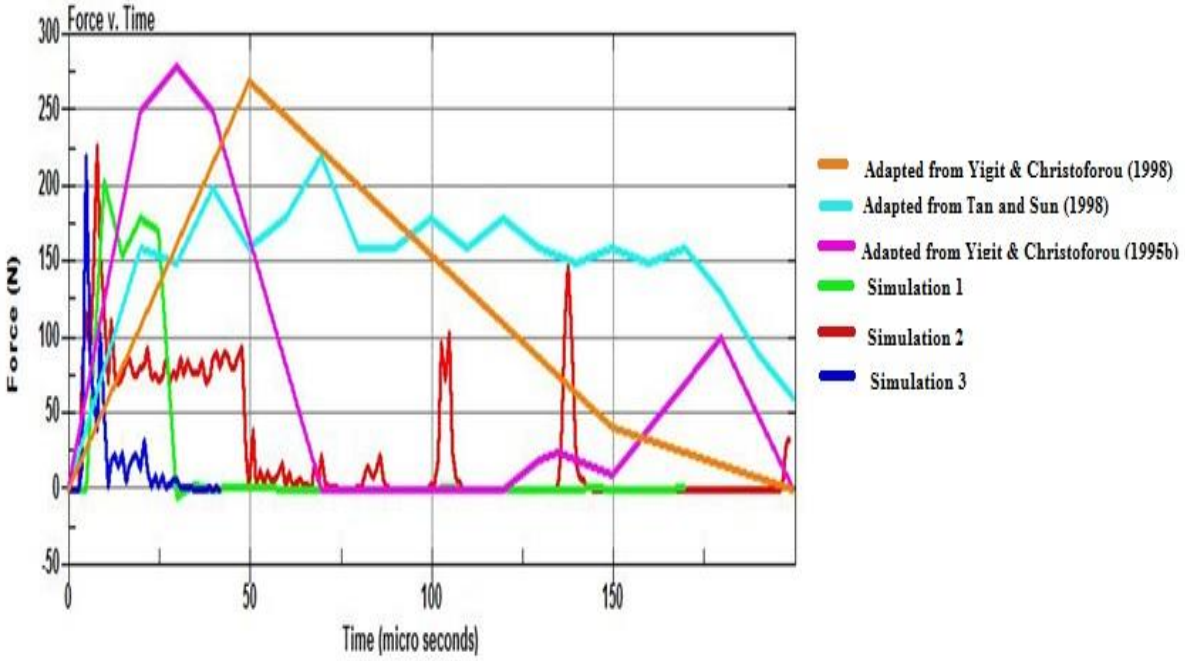

Figure 3: The force versus time graph for the simulations of T300/934 CFRP beam compared to the results from previous papers by Tan and Sun (1998), Yigit and Christoforou (1995b) and Yigit and Christoforou (1998).

Figure 3 shows the three different material model simulations against three different sets of previously found data. The first two are the analytical models from Yigit and Christoforou (1995b and 1998) for the beam and plate of the T300/934 CFRP which both used a spherical impactor. The results were compared against the plate impact model used by Tan and Sun (1998) which uses a pendulum mechanism with a hemispherical impact surface. The plate for this experiment was 152mm by 102mm and the impactor was a bullet shape of length 25.4mm with a hemispherical head of diameter 19.1mm and total weight 31.7g. The velocity in this experiment was 2.92 m/s. The impact force from this experiment was measured using a transducer fixed in the middle of the impactor. The magnitude of the maximum force from the three different models was 205 N for the composite failure model (simulation 1), 245 N for the composite damage model (simulation 3) and 255 N for the orthotropic elastic model (simulation 2). The maximum forces for the three models were 280 N for Yigit and Christoforou (1995b), 265N for Yigit and Christoforou (1998), and 250 N for Tan and Sun (1998). The models were 27%, 12.5% and 8.9% different from the analytical results of Yigit and Christoforou (1995b). This shows that the two material models that model the behaviour best are the orthotropic elastic material model and composite damage material model. These differences can again be partially accounted for by the use of mechanical properties from two sources which may not be 100% consistent due to the uncertainty in the exact fibre volume fraction and the arrangement of laminae, and the slightly different steel spherical impactor. These models behave very similarly before the failure criteria are exceeded. The original results from these sources are displayed in Appendix A. The force calculated by the simulation has much more noise in the results than the analytical solution. However, it has similar peaks to the analytical results after a longer time has passed (at the 140 microsecond mark compared to the 180 microsecond mark of the analytical results).

B. SE-84 GFRP Beam

The maximum displacement reached for the GFRP beam is 15.5mm. Given all the models showed similar trends, the simulation for the composite damage model only is shown in figure 4 (simulation 1). Since there was no previous data available for the SE-84 GFRP beams it was compared against the previous analytical results found in Yigit and Christoforou (1995b). This comparison was used for order of magnitude validation. Given that the impact was a lateral impact (i.e. in the transverse direction), the Young's modulus and other material properties related to this direction are largely dependent on the matrix material. It is shown in table 2 that these properties are reasonably similar for the GFRP beams and CFRP beams. The GFRP beam has a quicker restorative response with the displacement looking to return to 0mm from the 150 microsecond mark with a sharper gradient.

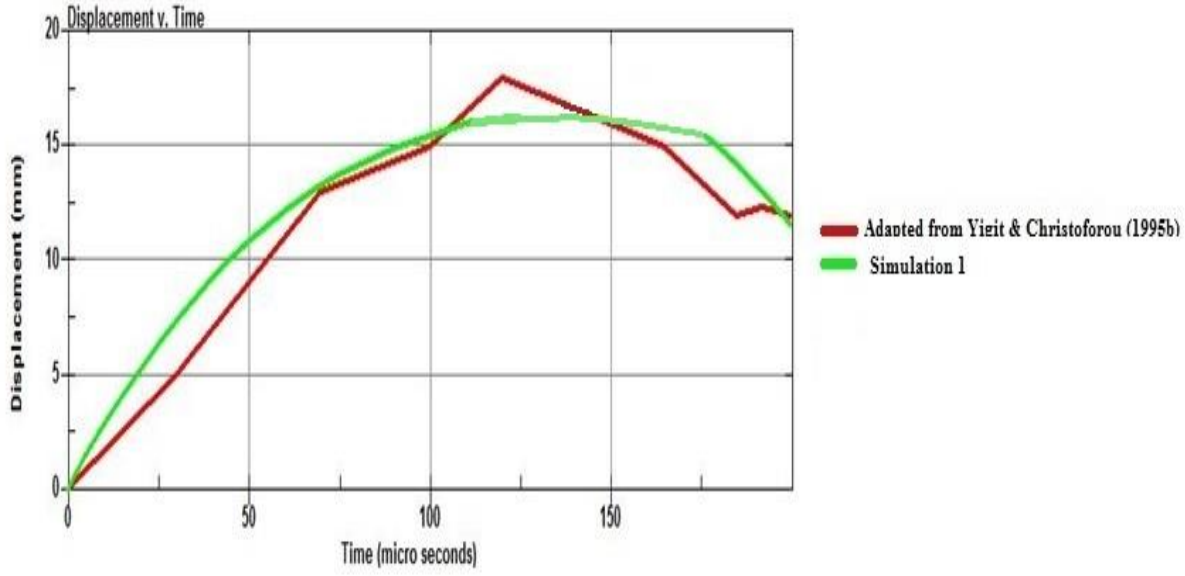

Figure 4: The displacement versus time curve comparing my simulation for the SE-84 GFRP beam to the data adapted from Yigit and Christoforou (1995b).

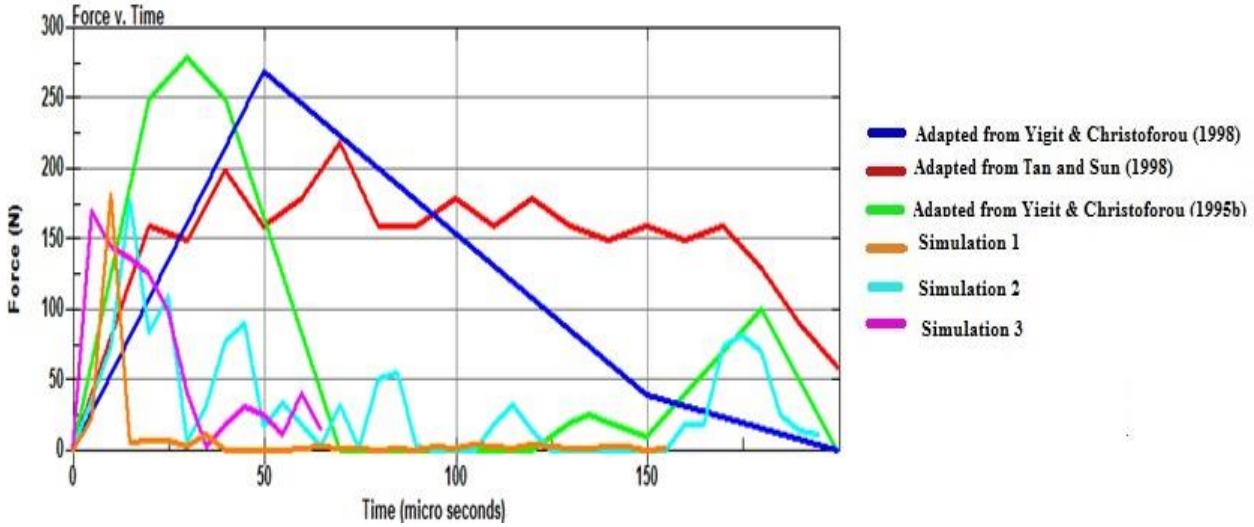

Figure 5: The force versus time graph for the simulations of SE-84 GFRP beam compared to the results from previous papers by Tan and Sun (1998), Yigit and Christoforou (1995b) and Yigit and Christoforou (1998)

The maximum forces measured in the simulations are 171N for the composite failure material model (simulation 3), 178N for the orthotropic elastic material model (simulation 2) and 183N for the composite damage material model (simulation 1). These results are all within less than 7% of the comparison data. This shows that for the low velocity used in the simulations, the models all predict the behaviour of the material accurately. Given the similar properties for the transverse direction when comparing the GFRP beam to the CFRP beam, the impact force is expected to be and is in a similar order of magnitude.

C. Comparison of T300/934 CFRP Beam and SE-84 GFRP Beam

The force on the CFRP beam is 245N and 255N (average 250N) whilst the GFRP beam is 171N, 178N and 183N (average 177.3N). The impact force has a much sharper rise in the CFRP beam than in the GFRP beam. The impact force on the CFRP beam is 29% greater than the impact force on the GFRP beam (calculated using the average values). Given the higher impact force on the T300/934 CFRP beam (as shown in figure 6) the Hertzian contact law (and the Hertz-Sveklo's Theory) predicts that the displacement (or deflection) is expected to be and is greater. The maximum displacement in the CFRP beam is 16.2mm compared to 15.5mm in the GFRP beam as shown in figure 7. The difference between the CFRP beam and GFRP beam is 4.3%. The factor that influences how force relates to displacement is the Hertzian stiffness (as shown in Eq. 4 and 10), which is dependent on the Young's modulus of the material for isotropic materials and a much more complicated formula of properties for orthotropic and anisotropic materials (that depends on a combination of the Young's and shear moduli). The

combination of the Young's and shear moduli that affects the Hertzian stiffness helps to account for the difference in percentages for force compared to displacement. Overall the higher the Hertzian stiffness, the lower the deflection is for a given force. Given the low velocity of the simulation the failure criteria for the composite damage model and composite failure models weren't exceeded and as such the different strengths of the materials and the post failure behaviour of the materials did not influence the simulation.

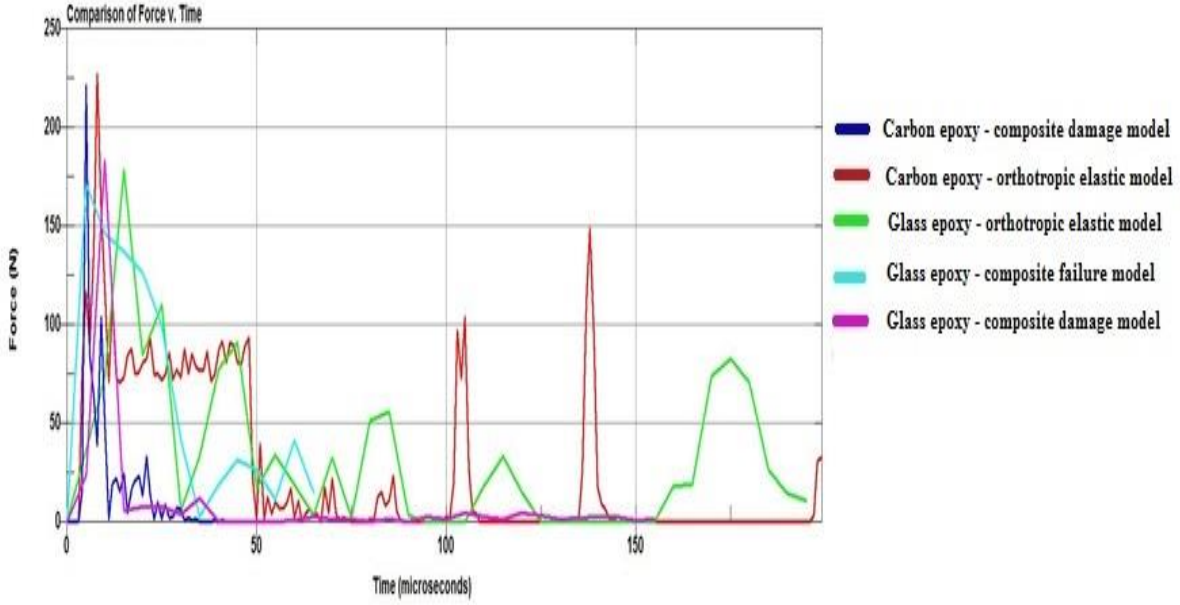

Figure 6: The force versus time graph for the comparison of the T300/934 CFRP beam compared to the SE-84 GFRP beam.

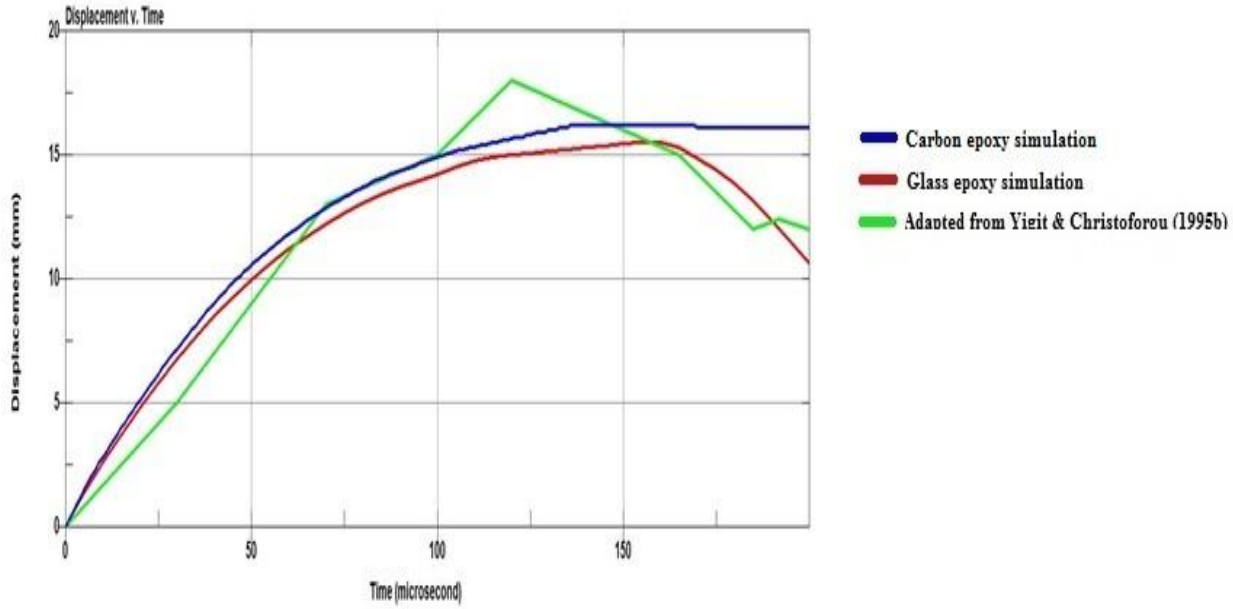

Figure 7: The displacement versus time graph for the comparison of the T300/934 CFRP beam compared to the SE-84 GFRP beam including the previous data from Yigit and Christoforou (1995b).

IV. Conclusion:

The simulation of T300/934 CFRP beam and SE-84 GFRP beam was conducted to expand the knowledge of how composite material beams behave under impact conditions. The increase of use of composites in a variety of applications requires us to also understand how the materials behave under unanticipated events such as impact. The use of simulation allows a cheaper and less time consuming method of predicting the behaviour for more complex structures under impact loading. As such this simulation study was conducted to predict the behaviour and compare the two materials. It was also conducted to see if an accurate simulation could be conducted to match previous analytical and experimental data. This helps to ensure the accuracy and validity of this simulation and any simulations conducted using these materials in the future (provided they are using the same material models). The low velocity impact of the steel sphere travelling at 3.0 m/s caused a maximum displacement of 16.2mm in

the CFRP beam and 15.5mm in the GFRP beam and an impact force of 250N in the CFRP beam and 177.3N in the GFRP beam. This data matched well against the previous results from Yigit and Christoforou (1995b) that were used to ensure the accuracy and validity of the models. The difference between the T300/934 CFRP beam simulation and previous experiment results was 10% for the displacement and 10.7% for the impact force. The results from the GFRP beam are expected to be in the same order of magnitude and reasonably similar to the CFRP beam results, given the similar transverse mechanical properties of these two materials. Out of the three different material models used for the three different simulations of the CFRP beam and GFRP beam (orthotropic elastic, composite damage and composite failure). The orthotropic elastic and composite damage models were the most accurate of the three models. These two models were very similar when comparing the behaviour they showed. The composite failure model did not model the behaviour of the CFRP and GFRP beams as accurately as the orthotropic elastic and composite damage model. Due to the low velocity impact either of these two models can be used to accurately simulate the physics behind the CFRP beam and GFRP beam.

V. Recommendation for Future Work

Future work for another project could also include more complicated geometric models. It could also include an experimental validation of the numerical models for these materials and boundary conditions.

Acknowledgements

I would like to acknowledge the guidance of Professor Evgeny Morozov, Professor Paul Hazell, Dr John-Leng Liow and Mr Alan Fien in the progress of this project and ensuring it covered the relevant areas. I would also like to acknowledge Mustafizur Rahman for his assistance with the LS-DYNA and ANSYS work in this project.

References:

Bisagni, C., Di Pietro, G., Fraschini, L. & Terletti, D., 2005, 'Progressive crushing of fiber-reinforced composite structural components of a Formula One racing car', *Composite structures*, vol. 68, no. 4, pp. 491-503.

Bucinell, R. B., Nuismer, R. J. & Koury, J. L., 1991 'Response of composite plates to quasi-static impact events', in Hahn, H. T., (Third Volume) *Composite Materials: Fatigue and Fracture*, ASTM STP 1110, ASTM, Philadelphia, PA, pp. 528-49.

Chang, F. K., & Chang, K. Y., 1987a, 'Post-failure analysis of bolted composite joints in tension or shear-out mode failure', *Journal of Composite Materials*, vol. 21, pp. 809-833.

Chang, F. K. & Chang, F. Y., 1987b, 'A Progressive Damage Model for Laminated Composite Containing Stress Concentrations', *Journal of Composite Materials* vol. 21, no. 9, pp. 834-855.

Duflou, J. R., De Moor, J., Verpoest, I., & Dewulf, W., 2009, 'Environmental impact analysis of composite use in car manufacturing', *CIRP Annals-Manufacturing Technology*, vol. 58, no. 1, pp. 9-12.

Johnson, K. L., 1985, *Contact Mechanics*, Cambridge University Press, Cambridge.

Khalili MR., 1992, 'Analysis of the dynamic response of large orthotropic elastic plates to transverse impact and its application to fibre reinforced plates', PhD Thesis, I.I.T. Delhi.

Khalili, S. M. R., Mittal R. K., & Mohammed Panah N. M., 2007, 'Analysis of fiber reinforced composite plates subjected to transverse impact in the presence of initial stresses', *Composite Structures*, vol. 77, pp. 263-268.

Kim Y., Davalos J. F., & Barbero E. J., 1996, 'Progressive Failure Analysis of Laminated Composite Beams', *Journal of Composite Materials*, vol. 30, No. 5, pp. 536 -560.

Mamalis, A. G., Robinson, M., Manolakos, D. E., Demosthenous, G. A., Ioannidis, M. B., & Carruthers, J., 1997, 'Crashworthy capability of composite material structures', *Composite structures*, vol. 37, no. 2, pp. 109-134.

Marsh, G., 2005, 'Airframers exploit composites in battle for supremacy', *Reinforced Plastics*, vol. 49, no. 3, pp. 26-32.

Matzenmiller, A. L. J. T. R., Lubliner, J., & Taylor, R. L., 1995, 'A constitutive model for anisotropic damage in fiber-composites', *Mechanics of materials*, vol. 20, no. 2, pp. 125-152.

Mines, R. A. W. & Alias, A., 2002, 'Numerical simulation of the progressive collapse of polymer composite sandwich beams under static loading', *Composites*, vol. 33, pp. 11-26.

Quilter, A., 2001, 'Composites in aerospace applications' *IHS White Paper*, 444, pp. 1-3.

Rahman, M 2013, 'Impact Resistance of Laminated Hybrid Composite Panels Composed of Compliant and Rigid Plies', PhD Thesis, University of New South Wales at Canberra.

Reddy, Y. S. N., & Reddy, J. N., 1992, 'Linear and non-linear failure analysis of composite laminates with transverse shear', *Composite Science and Technology*, vol. 44, pp. 227-255.

Santiuste, C., Sanchez-Saez, S., & Barbero, E., 2010, 'A comparison of progressive-failure criteria in the prediction of the dynamic bending failure of composite laminated beams', *Composite Structures*, vol. 92, pp. 2406-2414.

Schweizerhof, K., Weimar, K., Munz, T., Rottner, T., 1998, 'Crashworthiness Analysis with Enhanced Composite Material Models in LS DYNA Merits and Limits', *5th International LS DYNA User's Conference*.
Swanson, S., 1992, 'Limits of Quasi-Static Solutions in Impact of Composite Structures', *Composites Engineering*, vol. 2, no. 4, pp. 261-267.
Sveklo V. A., 1964, 'Boussinesq type problem for the anisotropic half-space', *Journal Applied Mathematics and Mechanics*, vol. 28, no. 1099–105.
Tan, T. M., & Sun, C. T., 1985, 'Use of statical indentation law in the impact analysis of laminated composite plates', *Journal of Composite Materials*, vol. 52, pp. 6-12.
Wu, H. T., & Springer, G. S., 1988, Measurements of Matrix Cracking and Delamination Caused by Impact on Composite Plates, *Journal of Composite Materials*, vol. 22, pp. 518-532.
Yigit, A. S. & Christoforou, A. P., 1994, 'On the impact of a spherical indenter and an elastic-plastic transversely isotropic half-space', *Composite Engineering*, vol. 4, pp. 1143-52.
Yigit, A. S. & Christoforou, A. P., 1995a, 'On the impact between a rigid sphere and a thin composite laminate supported by a rigid substrate', *Composite Structures*, vol. 30, pp. 169-77.
Yigit, A. S. & Christoforou, A. P., 1995b, 'Impact dynamics of composite beams', *Composite structures*, vol. 32, pp. 187-195.
Yigit, A. S. & Christoforou, A. P., 1998, 'Characterization of impact in composite plates', *Composite Structures*, No. 43 pp. 15-24.

Appendix:

Appendix A: Original comparison graphs.